Spectrochimica Acta Part A: Molecular and Biomolecular Spectroscopy 300 (2023) 122881

Contents lists available at ScienceDirect

Spectrochimica Acta Part A:
Molecular and Biomolecular Spectroscopy

journal homepage: www.journals.elsevier.com/spectrochimica-acta-part-a-molecular-and-biomolecular-spectroscopy

Highly sensitive cholesterol concentration trace detection based on a microfiber optic-biosensor enhanced specificity with beta-cyclodextrin film

Zifan Hou [a], Dandan Sun [a,b,*], Guanjun Wang [c], Jie Ma [a,b,*]

[a] School of Physics and Electronic Engineering, Shanxi University, Taiyuan, China
[b] Collaborative Innovation Center of Extreme Optics, Shanxi University, Taiyuan, China
[c] School of Information and Communication Engineering, Hainan University, Haikou 570228, China

HIGHLIGHTS

- A microfiber interferometer with poly-dopamine-β-CD membrane for cholesterol detection.
- Functional film using one-step immersion method.
- The sensor has high sensitivity, specific detection, and low temperature influence.
- The sensor can respond to 0.001–1 mM cholesterol with a sensitivity of 12.7 nm/(mM).

GRAPHICAL ABSTRACT

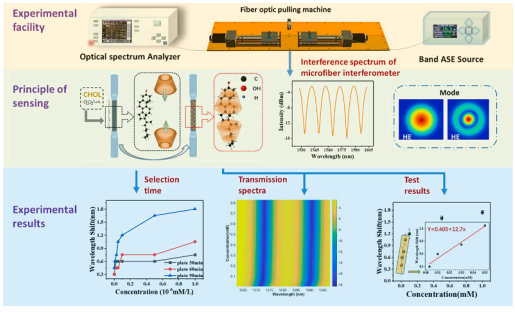

ARTICLE INFO

Keywords:
Cholesterol
Biosensor
β-cyclodextrin
Microfiber interferometer

ABSTRACT

A beta-cyclodextrin (β-CD) based optic-fiber microfiber biosensor for the detection of cholesterol concentration is propose and experimentally demonstrated. As an identifying substance, β-CD is immobilized on the fiber surface for cholesterol reaction to form an inclusion complex. When the surface refractive index (RI) change is cause because of capturing the complex cholesterol (CHOL), the proposed sensor translates RI change into a macroscopic wavelength drift in the interference spectrum. The microfiber interferometer has a high RI sensitivity of 1251 nm/RIU and a low-temperature sensitivity of −0.019 nm/°C. This sensor can rapidly detect cholesterol in the concentration range of 0.001 to 1 mM and has a sensitivity of 12.7 nm/(mM) in the low concentration range of 0.001 to 0.05 mM. Finally, the characterization by infrared spectroscopy shows that the sensor can indeed detect cholesterol. This biosensor has a few strong advantages of high sensitivity and good selectivity, which expects great potential in biomedical applications.

1. Introduction

Cholesterol, as a derivative of cyclopentane poly-hydro phenanthrene, is an essential substance in human tissues and plays an important role in cellular life to synthesize a variety of nutrients necessary for life [1]. However, excessive intake of substances containing cholesterol may lead to the development of diseases. For example, the consumption of eggs, meat products, and other foods rich in high cholesterol

* Corresponding authors at: School of Physics and Electronic Engineering, Shanxi University, Taiyuan, China.
E-mail addresses: sundd@sxu.edu.cn (D. Sun), mj@sxu.edu.cn (J. Ma).

https://doi.org/10.1016/j.saa.2023.122881
Received 14 January 2023; Received in revised form 10 May 2023; Accepted 11 May 2023
Available online 16 May 2023

concentration may lead to various diseases such as hypertension, heart disease, cerebral infarction, and coronary heart disease [2]. Therefore, it is necessary to improve the development of a low-cost and highly sensitive sensor for cholesterol detection.

Several methods exist at this stage for the detection and analysis of cholesterol, which include enzyme analysis methods [3], mass spectrometry [4], liquid chromatography [5], and gas chromatography [6]. Enzyme analysis methods require large amounts of enzymes that are expensive [3,7]. Mass spectrometry has good sensitivity, but the expenses of required reagents, consumables, and maintenance services for the instrument are high [8]. Liquid chromatography and gas chromatography can analyze organic compounds, but qualitative analysis is more difficult[356]. Through the above methods discussed, these methods have high accuracy, but the equipment is expensive and testing requires the production of a large number of samples. Therefore, there is a significant demand for a simpler, miniaturized, and inexpensive method to detect cholesterol concentration.

Nowadays, given its inexpensive, compactness, simple operation, and high sensitivity, an optic-fiber sensor is considered as an attractive option to provide a platform for cholesterol detection [8]. To date, different structures and methods for monitoring cholesterol concentration have been reported. Vivek Semwal et al. have fabricated localized and propagating surface-based plasma optic-fiber sensors for cholesterol detection using cholesterol oxidase [9]. Haitao Lin et al. have measured cholesterol concentration by immobilizing cholesterol oxidase at different temperatures to catalyze cholesterol[10]. Yi Lu et al. have used β-CD based reflective fiber-optic surface plasmon resonance sensor for cholesterol detection[11]. Niteshkumar Agrawal et al. have used gold nanoparticles and zinc oxide immobilized on core mismatch fiber structure to excite local surface plasmon resonance phenomena to detect cholesterol concentration [12]. Wanlu Zheng et al. have designed a plasmon resonance fiber optic biosensor to detect cholesterol concentration by wrapping β-CD on the surface of the sensor probe [14]. Yujuan Luo et al. have designed a tilted fiber-Bragg grating sensor for the detection of cholesterol solutions [14]. These results not only hold great potential for sensing specificity with the recognition element (cholesterol oxidase and β-CD) but also contribute to future studies on the practical early disease detection. As the promising material, β-CD is a class of cyclic oligosaccharides whose structural core consists of a size-stable hydrophobic cavity that can trap or package other molecules. Due to the distinctive hydrophilic outer surface and cyclodextrins, it can selectively wrap cholesterol to form stable inclusions by van der Waals forces, electrostatic attraction, and other interactions [15].Therefore, β-CD is finally selecte as the recognition molecule.

In this work, a tapered microfiber interferometer coate with a β-CD film can detect cholesterol concentration considering the sensitivity to external refractive index due to a strong evanescent field. This tapered interferometric structure of the sensor has the advantages of greater safety, simplicity of operation, high RI sensitivity, and wavelength demodulation [16]. The sensor has a high RI sensitivity of 1251 nm/RIU and a low-temperature cross-sensitivity of −0.019 nm/∘C. Experimental results show that cholesterol concentrations can be detected in the range of 0.001 to 1 mM, with a sensitivity of 12.7 nm/mM at low concentrations of 0.001 to 0.05 mM. By the loading of other biomolecules, the proposed sensor with stability and specificity can serve as a platform for diverse biochemical detections in the future.

2. Materials and methods

2.1. Reagents and instruments

Dopamine hydrochloride (98%), Tris-Hydrochloride (pH8.5), Cholesterol (99%), β-CD (98%), and Triton x-100 (biotech grade) are purchased from Shanghai Macklin Biochemical Co., Ltd. (Shanghai, China). During the experiment, β-CD is dissolved in deionized water (DI). The macroscopic structure of the microfiber interferometer is observed using an optical microscope (Caikon DMM-200C). Finally, the experimental samples are characterized by infrared spectroscopy (Nicolet iS50) to verify the absorption spectra of different substances.

Optical instruments used in an amplified spontaneous emission source (ASE, range 1528–1603 nm with 10 dBm power), an optical spectral analyzer (OSA, AnritsuMS9740A, range 600–1700 nm). The auxiliary instruments included a fusion splicer (Fujikura87S +), a taper pulled (ZOLIX MC600), a digital refractometer (Brix/RI-Chek Reichert), a temperature chamber (NG6000-2), etc.

2.2. Experimental setup and fabrication of microfiber interferometer

Fig. 1 shows the experimental setup including the fabricating microfiber interferometer. Light is emitted from an ASE source, transmitted to a microfiber interferometer, and then detected by an OSA with a wavelength resolution of 0.03 nm [17]. The microfiber interferometer is fabricated through a commercial optical fiber by heating with a hydrogen flame and stretching with a taper puller. The diameter of this fiber is gradually reduced from 125 μm to 8 μm by the heating method (automatically) [18]. To avoid errors, the operation parameters are set, which include the speed of each taper pull of 2 mm/s, the acceleration of 5 mm/s^2, the maximum speed of 9 mm/s, and the taper pulling distance of 18 mm. A microfiber interferometer with good stability is successfully prepared. Fig. 1(left) shows the schematic diagram of microfiber structure parameters, which is an isometric enlargement. A microfiber interferometer structure includes two transition regions with a length of about 3 mm and a uniform region at the waist with a length of 12 mm and a diameter of about 8 μm. These insets are real maps of each part of the tapered microfiber drawn by an optical microscope (Caikon DMM-200C).

2.3. Sensing principle

2.3.1. Principle of microfiber interferometer

When the first tapered transition zone to the waist area has fiber entry, a part of the core mode can couple into the envelope of the smaller diameter tapered region under the effect of the fading field, which will excite the higher-order modes in the envelope [19]. In the full-waist region, simultaneous propagation of basic core and cladding patterns, with the fundamental mode (HE_{11}) and the higher-order mode (HE_{12}) propagating mainly. Fig. 1 (right) shows the transverse electric field amplitude distribution of HE_{11} and HE_{12} for the main interference modes [1920]. Base core mode and cladding mode coupling when light propagates to the second conical transition region [21].

This structure of the fiber optic interferometer allows the coupling and recombination of modes and produces an interferometric pattern. In the transition region, the resulting coupling intensity is higher than that of the other higher-order states [18]. When the external refractive index changes, the interferometric wave appears blue shifted or redshifted, and the sensitivity at this point can be used to evaluate the refractive index performance of the sensor. It can be expressed as [2022].

$$\frac{d\lambda}{dR_{sm}} = \frac{\lambda}{\Gamma}\left(\frac{1}{\Delta R_{ccm}}\frac{d\Delta R_{ccm}}{dR_{sm}}\right) \tag{1}$$

where $\Gamma = 1 - \frac{\lambda}{\Delta R_{ccm}}\frac{d\Delta R_{ccm}}{d\lambda}$ is the factor of dispersion, the calculated value is a negative number. λ is the wavelength of the inclination angle in the transmitting spectrum, and R_{sm} is the RI of the surrounding medium. and $\frac{d\Delta R_{ccm}}{dR_{sm}}$, $\frac{d\Delta R_{ccm}}{d\lambda}$ are the changes in the index dependence induced under the conditions of very small changes in RI of external refractive index effect, and wavelength, respectively. According to Formula (1), Because the exponential increment of the HE_{12} mode is larger than that of the HE_{11} mode as the external RI increases, the microfibers with small diameter and index differences have high sensitivity [22]. ΔR_{ccm} is the distinction between the effectiveness of the core mode and the cladding mode. R_{co} and R_{cl} are the RI of the microfiber core and cladding. The relationship

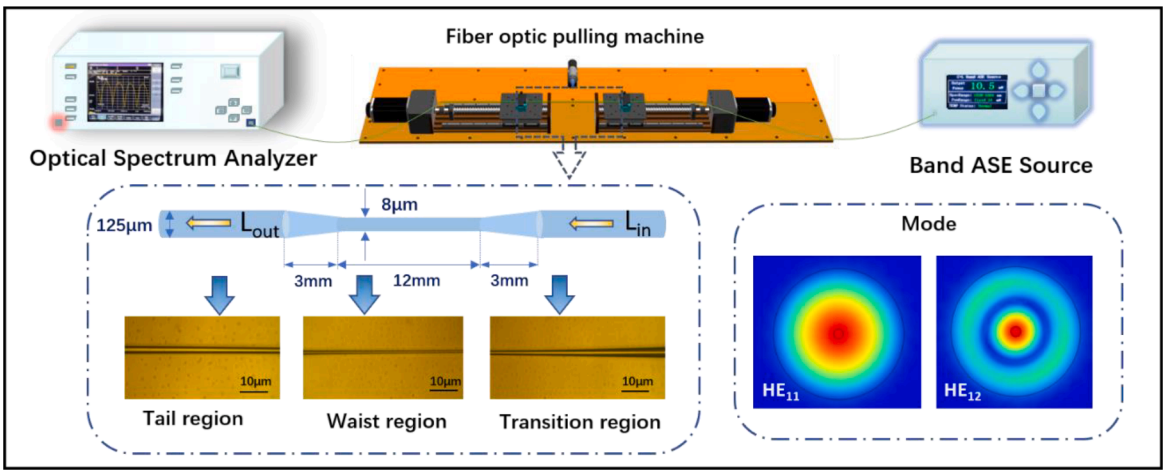

Fig. 1. Test system experimental setup and fabrication of silicon microfiber interferometer. (Inset: the transverse electric field amplitude distribution of HE_{11} and HE_{12} under the main interference modes.

between them can be expressed as

$$\Delta R_{ccm} = R_{co} - R_{cl} \tag{2}$$

$$d\Delta R_{ccm} = \Delta R_{ccm2} - \Delta R_{ccm1} \tag{3}$$

As pointed out by finite element analysis software, $\lambda = 1565.05$ nm, and the directivity of the surrounding air$R_{sm} = 1$. When the index difference of ΔR_{ccm} increases under the influence of a small change in wavelength or refractive index of the surrounding air, the index increment of the HE_{12} mode is larger than that of the HE_{11} mode, so $\frac{d\Delta R_{ccm}}{dR_{sm}}$ is negative and the discrete factor Γ is also negative. The results show that the wavelength shifts red with increasing RI. Most importantly, the wavelength is red-shifted with increasing RI of the external surrounding medium [20].

2.3.2. *Principles of biosensor detection*

PDA is formed by a combination of physics and chemistry, as shown in Fig. 2(a) [23]. The oxidation of dopamine (DA) to dopamine quinone dopamine can polymerize and form PDA nanofilms with superb adhesion on the surface of geometric materials by oxidative polymerization of covalent bonds or physical self-assembly of dopamine. under weak alkaline conditions (pH 8.5). This enables superb adhesion on various material surfaces [24]. The most relevant reasons for the super-adhesive properties of PDA are the presence of catechol functional groups that can form covalent or non-covalent bonds (hydrogen bonds, van der Waals

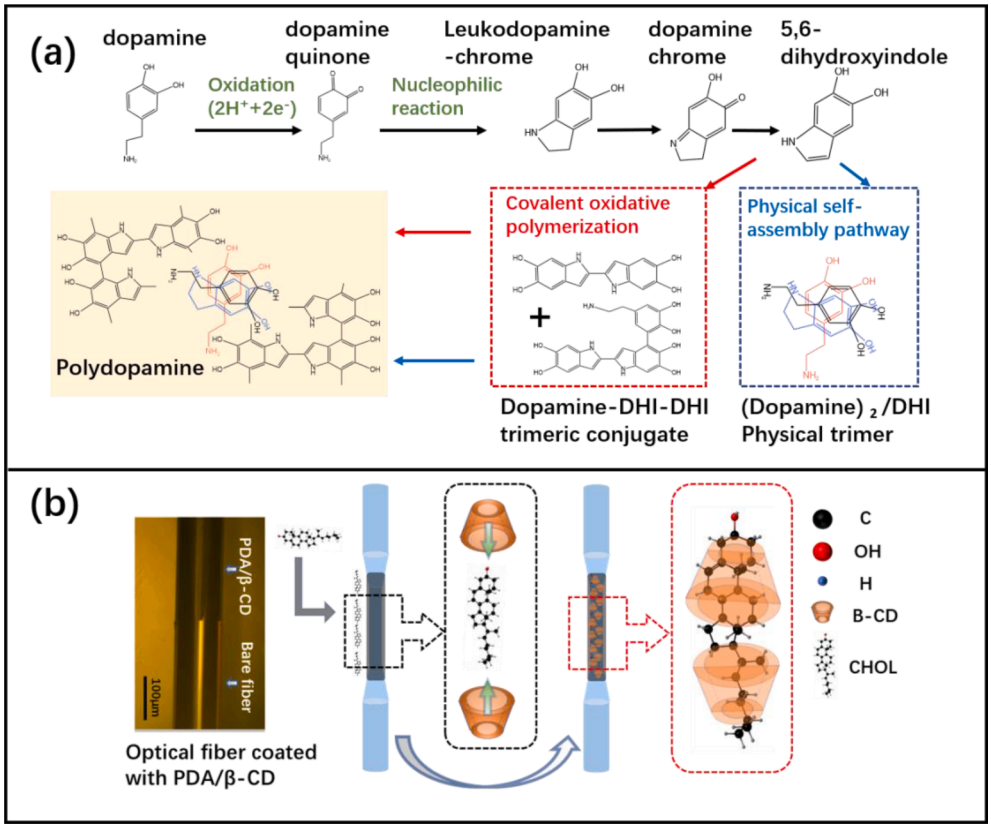

Fig. 2. Biofiber sensor detection principle. (a) Synthesis of polydopamine (PDA). (b) Schematic diagram of β-CD binding to cholesterol.

forces, or stacking forces) with the surface of the substrate material [25]. Therefore, β-CD can also be attached to PDA, and the combination of both can be attached to the specific microfiber biological probe.

A schematic diagram of the principle of cholesterol detection by the biological probe is shown in Fig. 2(b). The real picture of the single-mode fiber with the attached PDA/β-CD mixture in 90 min is shown in Fig. 2(b, left). The attachment is observed on the optical fiber with an optical microscope. It can be seen that the part attached by PDA/β-CD film is black, and the part not attached is the original color of the fiber. The initial fabrication of the sensor is completed.

β-CD is a group of cyclic oligosaccharides produced by the action of cyclodextrin glucosyltransferase on starch[26]. As shown in Fig. 2(b, middle), β-CD is shaped like a conical columnar hollow barrel with a wide caliber at one end and a narrow caliber at the other end and a cavity in the middle, which is the basis for β-CD to form an envelope [27]. All the secondary hydroxyl groups are arranged at the large mouth end of the conical column and the primary hydroxyl groups are arranged at the small mouth end, which gives them a certain hydrophilic appearance. As it is illustrated in Fig. 2(b, right), the most important feature of β-CD is its ability to encapsulate organic, inorganic, or gaseous molecules within the molecular cavity to form an encapsulant. This form can exist not only in the solid state but also in water and some organic solvents to form inclusion [28]. The common one is that β-CD can bind to CHOL to form inclusion complexes [29]. Because the molecules of CHOL are relatively large, they can only enter from the wide mouth end of β-CD forming the inclusion complex, while the hydroxyl group on the tail extends from the narrow mouth end of β-CD. The structure of β-CD and cholesterol inclusion complex is shown in Fig. 2(b, right). It can be seen that two β-CD molecules bind one cholesterol molecule, which is connected in a head-to-head manner [29].

3. Results and discussion

3.1. The performance of microfiber interferometer

Fig. 3 (a, left) shows the interference spectrum of the microfiber interferometer, and in this experiment, the main data comes from the last two dips. The data processing results of Fig. 3(a, right) show the response of the interferometer to RI and temperature.

These RI values of solutions are measured by a digital refractometer with an accuracy of 0.0002 to determine the simulated refractive index values of 1.3394–1.3687. Fig. 3 (a, right, red line) shows the RI sensitivity of 1251 nm/RIU with the interferometric wave gradually red-shifting during the experiment. The experimental procedure is carried out in a temperature chamber. The temperature response is obtained experimentally in a resistance furnace at 30–90 °C. As the temperature increases, the interference wave is gradually blue-shifted, and Fig. 3 (a, right, blue line) shows a temperature response sensitivity of −0.019 m/°C.

3.2. Fabrication of biological probe with β-CD

During the experiment, dopamine hydrochloride (DA) is dissolved with Tris-hydrochloride. Pipette 2 mL of Tris-Hydrochloride in a beaker and add 10 mg of DA to the beaker. Make up a DA solution with a concentration of 5 mg/mL. The solution is stirred for 30 min at room temperature, and in this process, the dopamine is gradually polymerized to reflect a gradual change from colorless to black. After that, take 10 mg of β-CD dissolved in 2 mL of deionized water, and stirred for 2 min at room temperature to fully dissolve β-CD, (at this time the β-CD is saturated). Let it stand for 5 min, and take the above clear liquid and add it to the just stirred PDA solution and continue to stir for 10 min to obtain PDA/β-CD functional film (polydopamine connecting with β-cyclodextrin).

In the experimental stage, to choose the best coating time, the prepared solution is coated on the microfiber interferometer for 30 min, 60

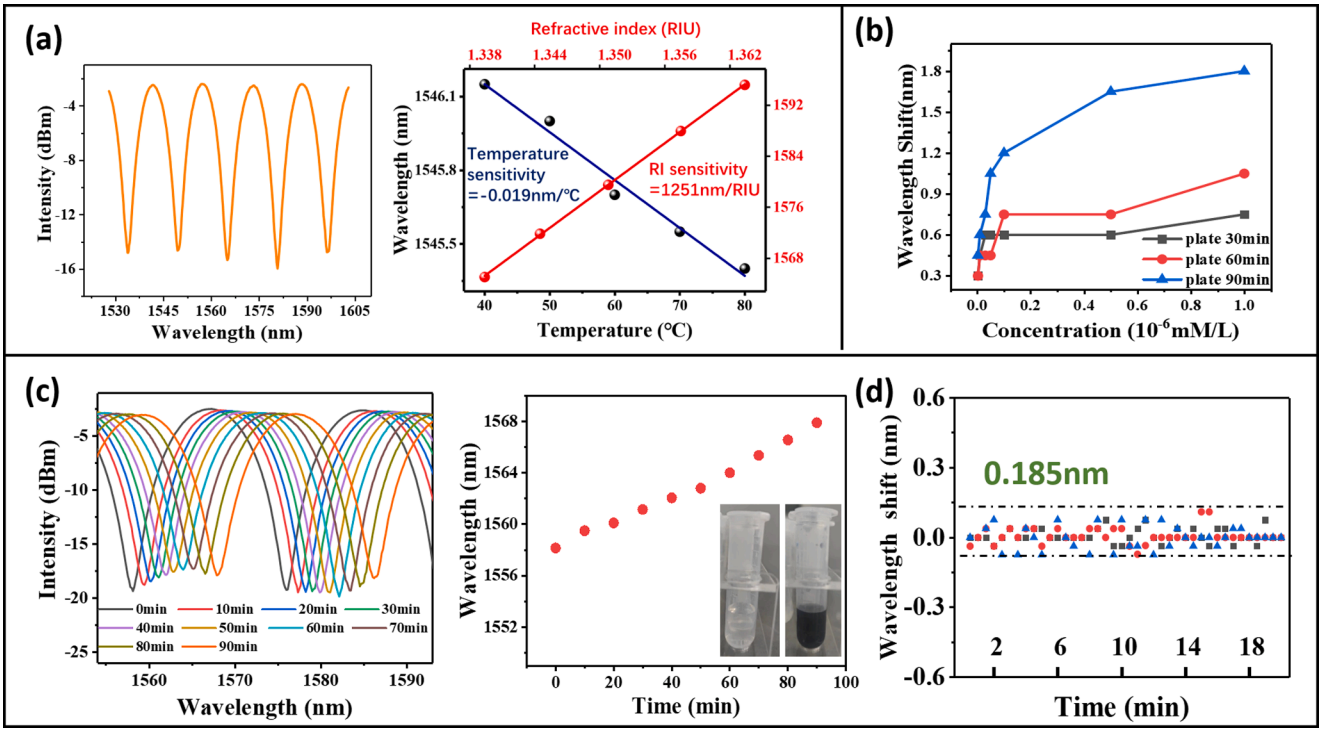

Fig. 3. (a) Interference spectrum of microfiber interferometer. Relationship between wavelength response RI and temperature fluctuations of silicon dioxide microfiber interferometer. (b) Selection of 90 min as the optimal coating time. (c) The functional films coating experimental result. (d) Results of three stability experiments.

min, 90 min, and then the cholesterol CHOL assay is detected by β-CD bioprobe, and the experimental results are shown in Fig. 3(b). The results show that the microfiber interferometer after 90 min coating could detect a larger concentration of cholesterol and the sensitivity is also the highest at this time, so 90 min is finally chosen as the coating time, and the biological microfiber probe with β-CD is successfully made. And in the concentration range of 0.001 to 0.03 mM, it can be seen that the sensitivity obtained by 90 min coating time is also the highest. while the other times, only low concentrations of CHOL could be detected, but no high concentrations of cholesterol could be accurately detected. Thus, 90 min is finally chosen as the coating time.

During the coating process, the change in the interference wave is recorded with a spectrometer. As shown in the left side of Fig. 3(c), the wavelength is regularly red-shifted by 10 nm. Fitting the data to Fig. 3(c, right), it can be observed that the wavelength is linearly related to time. The inset shows a real picture of the unpolymerized DA and the PDA obtained by stirring for 30 min, you can see the dark black matter. After successfully preparing the biological probe with β-cyclodextrin, it is washed with DI for 20 min to verify the stability, The results are shown in the Fig. 3(d). During the cleaning of the sensor, the interference spectrum did not change significantly, and the error fluctuation is 0.185 nm. Finally, a well-stabilized β-CD sensor is fabricated and used for the next detection experiments.

3.3. Detection of cholesterol

During the experiment, CHOL solutions of 0.001, 0.003, 0.01, 0.03, 0.05, 0.1, 0.5, and 1 (The unit of mM) concentrations are first prepared. In detail, 38.9 mg of cholesterol is first dissolved in 1 mL of Triton x-100 solution, which is stirred for 3 h at room temperature and then diluted with deionized water to the final concentration [11]. The cholesterol is detected with a fiber optic microfiber sensor starting from small concentrations and for 10 min at each concentration, and the interference wave at the final stabilization is selected as the most important data for the study. The transmission spectra in different CHOL concentrations are shown on the side of Fig. 4(a, left). It can be seen from the figure that the redshift in wavelength occurs with increasing concentration. The wavelength spectrum is further enlarged in the side of Fig. 4(a, right), which shows the wavelength shift data points with concentration during the detection process, and the wavelength gradually redshifts 1.8 nm with increasing concentration. To prove that the experimental results aren't accidental, each experiment is repeated three times with the error bar analysis. The relationship between concentration at 0.001 to 1 mM and wavelength are shown in Fig. 4(b), and the first four points are fitted obtained as shown in the inset of Fig. 4(b) with the fitted sensitivity of 12.7 nm/mM.

3.4. Specific characteristics

Specific response of the sensor to measure the object is an important criterion. To verify the specificity of the sensor, this biosensor is used to detect cholesterol by performing three tests on different substances in the same concentration range (0.001 to 1 mM). Fig. 5 shows the response of the β-CD biosensor to five different substances. The results show that Fatty alcohol, Vitamin D3, Oestrone, Stigmasterol, Folic acid, and Glucose shift by 0.1 nm, 0.35 nm, 0.35 nm, 0.05 nm, −0.2 nm, 0.1 nm while Cholesterol Blue shifts by 1.8 nm. This indicates that the response of the biosensor to cholesterol is much higher than that of the other substances, and the sensor has good specificity for cholesterol. the response is much higher than that of other substances, and the specific recognition of the cholesterol is good. Table 1 shows the different structures of the sensor to detect cholesterol. In comparison, our sensor is simple to fabricate, stable and sensitive.

3.5. Sensor characterization

To elucidate the interaction between the components in the fiber, we do Scanning Electron Microscope (SEM) to visualize the characteristics of the fiber surface. Ultraviolet visible light (UV–vis) spectroscopy to identify the binding of cholesterol to PDA/β-CD. Infrared spectroscopy to determine the composition of the fiber. Nuclear Magnetic Resonance (NMR) is used to determine the binding mode of β-CD/CHOL.

Fig. 6(a) shows the SEM image of the fibers. The Fig. 6(a, top) is the SEM image of the bare fiber showing the smooth fiber surface. When the fibers are immersed in the solution of PDA/β-CD for 90 min, it can be observed that the fiber surface is covered with uniform particles as shown in Fig. 6(a, middle). When the PDA/ β-CD attached fibers are tested for cholesterol, an increase in the particles attached to the fibers could be seen, as shown in Fig. 6 (a, bottom).

To demonstrate that the β-CD biological optic probe detects cholesterol, infrared spectra are analyzed on slides coated with PDA, PDA/β-CD, and PDA/β-CD/CHOL. In the infrared spectrum on the left side of

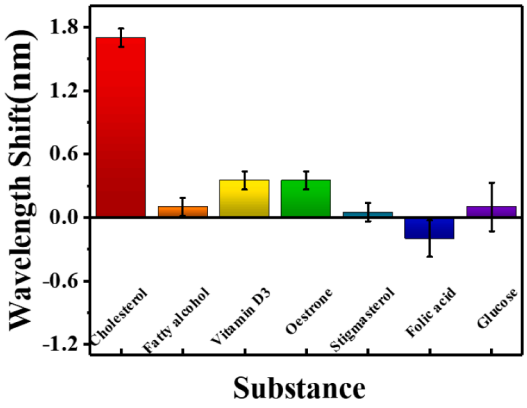

Fig. 5. This biosensor specific response to different substances (Fatty alcohol, Vitamin D3, Oestrone, Stigmasterol, Folic acid, Glucose).

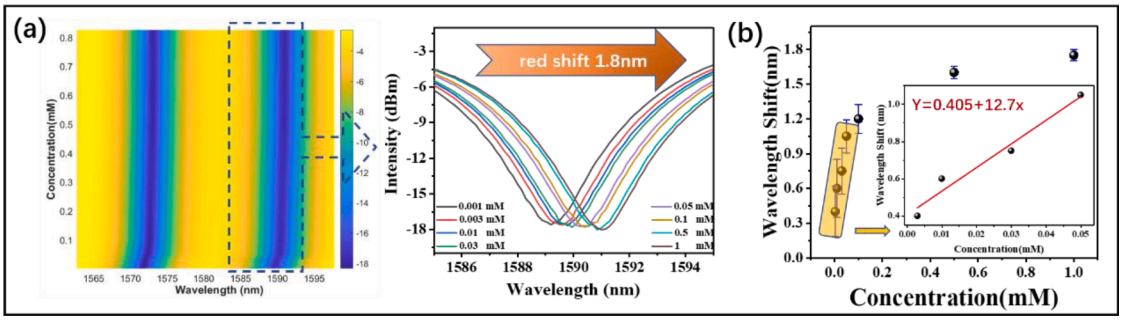

Fig. 4. Diagram of cholesterol detection (a)Transmission spectra and local magnification of CHOL detection by the biological probe (b)Error bar analysis of three experiments for the detection of cholesterol by β-CD.

Table 1
The different structures of the sensor to detect cholesterol.

Structure and material	Connector identification element	Concentration range	Sensitivity	Cost	Manufacturing difficulty	Publication date	Reference
Local and propagating surface plasma fiber optic sensor	cholesterol oxidase	0 to 10 mM	5.14 nm/mM	medium	medium	2018	[9]
Fiber optic sensor catalysis to the oxidation of cholesterol	cholesterol oxidase	0.5 to 6.7 mM	–	medium	easy	2019	[10]
Optical fiber surface reflection-structured plasma resonance sensor	Beta-cyclodextrin	0 mM to 0.05x10^{-3}mM	0.16 nm/mM	medium	medium	2020	[11]
Core mismatch optic-fiber sensor localized surface plasmon resonance	Cholesterol oxidase	0.1 to 10 mM	0.7 nm/mM	high	difficulty	2020	[12]
Plug-and-play surface plasmon resonance two-parameter optic-fiber biosensor	Beta-cyclodextrin	0 to 300x10^{-6} mM	0.012 nm/mM	high	difficulty	2022	[13]
Tilting Fiber Bragg Grating Sensor	none	0.0517 to 1.0344 mM	0.031 nm/mM	high	difficulty	2022	[14]
A β-CD-based fiber optic biosensor for the detection of cholesterol concentration	PDA/β-CD	0.001 to 1 mM	12.7 nm/mM	low	easy	2022	This work

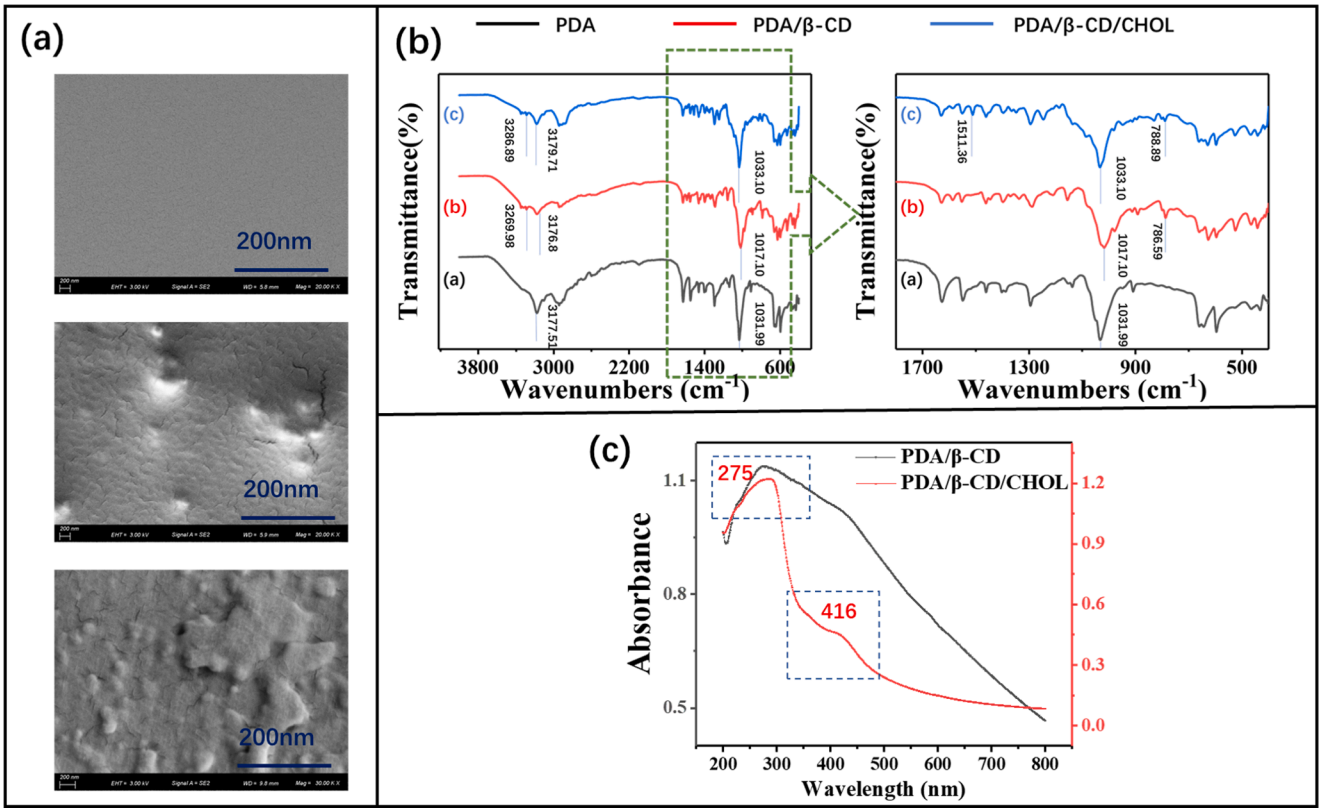

Fig. 6. (a) Scanning electron microscope images at a magnification of 20,000x. (b) Infrared spectra of PDA, PDA/β-CD, and PDA/β-CD/CHOL. The right side is a magnified view of the wavelength at 1750–250 cm^{-1}. (c) UV–vis spectra of PDA/β-CD and PDA/β-CD/CHOL.

Fig. 6(b), the absorption peaks at 3269–3287 cm^{-1} are the stretching vibration of –OH in β-CD and the stretching vibration of the conversion of –NH_2 to –NH on dopamine[30], and the quantitative absorption peak of β-CD near the absorption peak near 788 cm^{-1}, which is caused by the characteristic absorption of the ring vibration of β-CD[3031]. The absence of this peak in the infrared spectrum of PDA proves that β-CD is bound to PDA. The absorption peaks at 3176–3179 cm^{-1} and 1017–1034 cm^{-1} are C–H stretching vibrations and the stretching vibrations of C-O[31]. In the infrared spectrum in the Fig. 6(b, right), 1511.36 cm^{-1} is the H-O–H bending vibration of cholesterol [32], but this absorption peak is not present in the infrared spectra of PDA, PDA/β-CD. This proves that there is cholesterol bound in β-CD.

The Uv–vis spectra of PDA/β-CD and PDA/β-CD/CHOL in the range of 200–800 nm are shown in Fig. 6 (c). It can be seen that a strong absorption peak exists in the range around 275 nm for both PDA/β-CD and PDA/β-CD/CHOL, which is caused by the absorption of light by PDA/β-CD[3334]. And then, it can observe that only an absorption peak (near 416 nm) exists in the red line, which is caused by the absorption of light from cholesterol. It can demonstrate the binding of β-CD and CHOL.

To elucidate the interaction between the components in the fiber, we made Liquid NMR to illustrate the binding mode between them. Fig. 7(a) shows the H-NMR of β-CD, β-CD/CHOL in the range of 8–2 ppm, the red line indicates the H-NMR of β-CD/CHOL, and the black line indicates the H-NMR of β-CD. It is obvious from Fig. 7(a)(b) that the red line has 5 more peaks than the black line, which are 7.71 ppm, 6.78 ppm, 1.58 ppm, and 1.25 ppm. 0.63 ppm, where 7.17 ppm is the signal of the cholesterol proton H bond and 6.78 ppm is the signal of the cholesterol

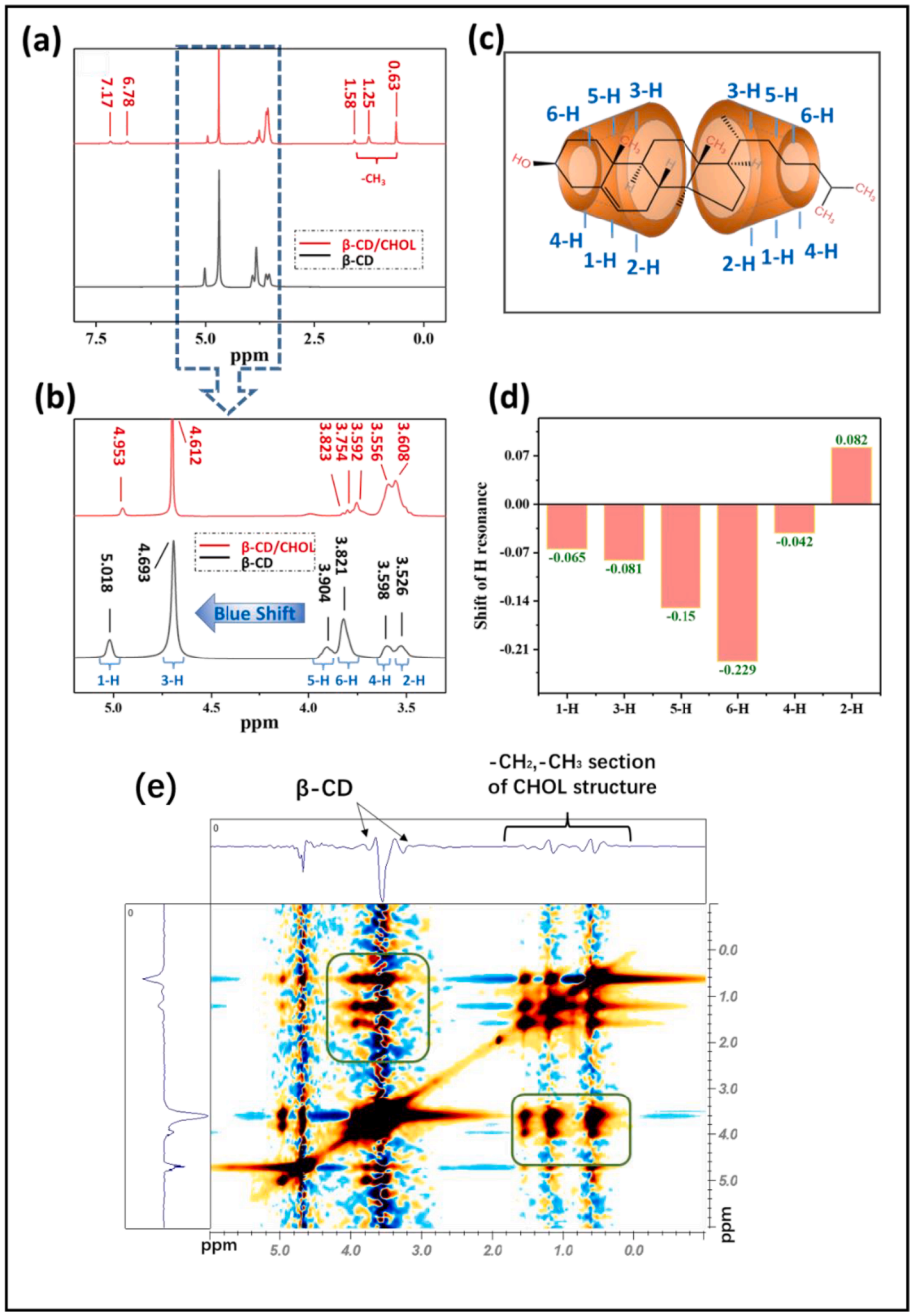

Fig. 7. (a) H-NMR of β-CD and β-CD/CHOL in the range of 8–2 ppm (b) Amplified H-NMR β-CD and β-CD/CHOL spectra in the range of 5.5–3 ppm (c) β-cyclodextrin proton signal shift map (d)H-NMR chemical shift of β-CD in the presence of cholesterol (solvent is tritium oxide) (e)NOESY spectra of β-CD/CHOL in D2O.

–OH bond. The cholesterol fraction is poorly decomposed due to the limited solubility of the linker in water. Thus, in the range of about 1.58 to 0.63 ppm, three peaks can be seen, which is partly the signal of cholesterol-CH_3. H-NMR data show a change in the proton signal of the CHOL fraction and the β-CD molecule. To illustrate the proton specific changes, an enlarged spectrum of H-NMR in the range of 5.5–3 ppm is added, as shown in Fig. 7(b), and this part is the signal of β-CD, from which it is seen that each proton signal is shifted and most of the proton signal of β-CD is moving out of the field. The position of the proton signal corresponding to each peak is shown in Fig. 7(c) [3536]. Protons 1-H, 2-H, and 4-H are located outside the lumen of β-CD, and protons 3-H, 5-H, and 6-H are located outside the lumen of β-CD. To facilitate the calculation, we counted the specific ppm of each proton signal shift, as shown in Fig. 7(d). From the figure, it can be seen that the proton signals belonging to the positions of 3-H, 5-H, and 6-H on the inner surface of β-CD are most obviously shifted, while the 1-H and 4-H signals located on the outer surface of the cavity are also shifted to the outside of the field, while the 2-H located on the outer surface of the hydroxyl group is shifted to the inside of the field. The shift of proton H proves that there are CHOL molecules entering the β-CD cavity. For β-CD, mainly the primary (6-H) and secondary hydroxyl groups (3)-H) are shifted. The shift of polycrystals belonging to the secondary hydroxyl group is about −0.081 ppm, while the shift of polycrystals belonging to the primary hydroxyl group is about −0.229 ppm. This proves that cholesterol molecules did enter the lumen of β-CD.

To characterize the binding mode (2:1) in the structure of cholesterol and β-CD, the nuclear overhauser effect spectroscopy (NOESY) H spectrum of β-CD/CHOL is tested [36]. The spectrum of the formation is shown in Fig. 7(e). In detail, the binding of the two β-CD porous fractions (3.4 to 3.9 ppm) and one CHOL (0.7 to 1.4 ppm) is exhibited. In Fig. 7(e,

right), mainly the –CH3 group can form an inclusion complex in D_2O for the proton of the cholesterol structure. The NOESY H spectrum in Fig. 7 (e) describes the binding mode (2:1) between β-CD and CHOL.

4. Conclusion

In this paper, a tapered microfiber interferometer based on PDA/β-CD functional film is proposed to detect the cholesterol concentration. The microfiber interferometer has a high RI sensitivity (1251 nm/RIU) and a low temperature cross-sensitivity (-0.019 nm/∘C). The sensor can detect cholesterol concentrations in the range of 0.001 to 1 mM. This sensor has a sensitivity of 12.7 nm/mM in the concentration range of 0.001 to 0.05 mM and can respond rapidly in the concentration range of 0.001 to 1 mM. Meanwhile, the proposed sensor has the stability and specificity. This method not only provides a new method for the determination of cholesterol concentration but also provides new ideas for his application in biomedical and other fields.

Declaration of Competing Interest

The authors declare that they have no known competing financial interests or personal relationships that could have appeared to influence the work reported in this paper.

Data availability

Data will be made available on request.

Acknowledgments

This work was supported by National Natural Science Foundation of China (62005147, 62175054); International Cooperation and Exchange of the National Natural Science Foundation of China (62020106014).

References

[1] S. Berger, G. Raman, R. Vishwanathan, P.F. Jacques, E.J. Johnson, Dietary cholesterol and cardiovascular disease: a systematic review and meta-analysis, Am. J. Clin. Nutr. 102 (2) (2015) 276–294, https://doi.org/10.3945/ajcn.114.100305.

[2] A.K. Basu, P. Chattopadhyay, U. Roychoudhuri, R. Chakraborty, Development of cholesterol biosensor based on immobilized cholesterol esterase and cholesterol oxidase on oxygen electrode for the determination of total cholesterol in food samples, Bioelectrochemistry 70 (2) (2007) 375–379, https://doi.org/10.1016/j.bioelechem.2006.05.006.

[3] B. Paital, A modified fluorimetric method for determination of hydrogen peroxide using homovanillic acid oxidation principle, Biomed Res. Int. 2014 (2014), 342958, https://doi.org/10.1155/2014/342958.

[4] H. Hidaka, N. Hanyu, M. Sugano, K. Kawasaki, K. Yamauchi, T. Katsuyama, Analysis of human serum lipoprotein lipid composition using MALDI-TOF mass spectrometry, Ann. Clin. Lab. Sci. 37 (3) (2007) 213–221, https://doi.org/0091-7370/07/0300-0213.

[5] A. Daneshfar, T. Khezeli, H.J. Lotfi, Determination of cholesterol in food samples using dispersive liquid-liquid microextraction followed by HPLC-UV, J. Chromatogr. B Anal. Technol. Biomed. Life Sci. 877 (4) (2009) 456–460, https://doi.org/10.1016/j.jchromb.2008.12.050.

[6] M. Beggio, C. Cruz-Hernandez, P.A. Golay, L.Y. Lee, F. Giuffrida, Quantification of total cholesterol in human milk by gas chromatography, J. Sep. Sci. 41 (8) (2018) 1805–1811, https://doi.org/10.1002/jssc.201700833.

[7] F.Z. Stanczyk, N.J. Clarke, Advantages and challenges of mass spectrometry assays for steroid hormones, J. Steroid Biochem. Mol. Biol. 121 (3–5) (2010) 491–495, https://doi.org/10.1016/j.jsbmb.2010.05.001.

[8] M. Lobry, D. Lahem, M. Loyez, M. Debliquy, K. Chah, M. David, C. Caucheteur, Non-enzymatic D-glucose plasmonic optical fiber grating biosensor, Biosens. Bioelectron. 142 (2019) 111506, https://doi.org/10.1016/j.bios.2019.111506.

[9] V. Semwal, B.D. Gupta, LSPR- and SPR-Based Fiber-Optic Cholesterol Sensor Using Immobilization of Cholesterol Oxidase Over Silver Nanoparticles Coated Graphene Oxide Nanosheets, 18, 1039–1046, IEEE Sens. J. (2018), https://doi.org/10.1109/jsen.2017.2779519.

[10] H. Lin, M. Li, L. Ding, J. Huang, A Fiber Optic Biosensor Based on Hydrogel-Immobilized Enzyme Complex for Continuous Determination of Cholesterol and Glucose, Appl. Biochem. Biotechnol. 187 (4) (2019) 1569–1580, https://doi.org/10.1007/s12010-018-2897-x.

[11] Y. Lu, H. Li, X.L. Qian, W.L. Zheng, Y. Sun, B.F. Shi, Y.N. Zhang, Beta-cyclodextrin based reflective fiber-optic SPR sensor for highly-sensitive detection of cholesterol concentration, Opt. Fiber Technol. 56 (2020) 102187, https://doi.org/10.1016/j.yofte.2020.102187.

[12] N. Agrawal, B. Zhang, C. Saha, C. Kumar, X. Pu, S. Kumar, Ultra-Sensitive Cholesterol Sensor Using Gold and Zinc-Oxide Nanoparticles Immobilized Core Mismatch MPM/SPS Probe, J. Lightwave Technol. 38 (2020) 2523–2529, https://doi.org/10.1109/JLT.2020.2974818.

[13] W.L. Zheng, Y.N. Zhang, L.K. Li, X.G. Li, Y. Zhao, A plug-and-play optical fiber SPR sensor for simultaneous measurement of glucose and cholesterol concentrations, Biosens. Bioelectron. 198 (2022) 113798, https://doi.org/10.1016/j.bios.2021.113798.

[14] Y.J. Luo, J.H. Luo, N. Wei, L. Ma, E. Liu, Experimental research on cholesterol solution concentration sensing based on tilted fiber Bragg grating, Optoelectron. Lett. 11 (2021) 661–664, https://doi.org/10.1007/s11801-021-1030-5.

[15] F. Fang, X.J. Huang, Y.Z. Guo, X. Hong, H.M. Wu, R. Liu, Selective and Regenerable Surface Based on β-Cyclodextrin for Low-Density Lipoprotein Adsorption, Langmuir: The ACS J. Surf. Colloids 34 (28) (2018) 8163–8169, https://doi.org/10.1021/acs.langmuir.8b00883.

[16] H. Jun, P.P. Zhang, M.S. Li, P.F. Zhang, L.Y. Ding, Complex of hydrogel with magnetic immobilized GOD for temperature controlling fiber optic glucose sensor, Biochem. Eng. J. 114 (2016) 262–267, https://doi.org/10.1016/j.bej.2016.07.012.

[17] S.H. Girei, H.N. Lim, M.Z. Ahmad, M.A. Mahdi, A.R. Md Zain, M.H. Yaacob, High Sensitivity Microfiber Interferometer Sensor in Aqueous Solution, Sensors 20 (17) (2020) 4713, https://doi.org/10.3390/s20174713.

[18] V. Ahsani, F. Ahmed, M. Jun, C. Bradley, Tapered Fiber-Optic Mach-Zehnder Interferometer for Ultra-High Sensitivity Measurement of Refractive Index, Sensors 19 (7) (2019) 1652, https://doi.org/10.3390/s19071652.

[19] V. Bhardwaj, D.K. Kishor, A. Sharma, Tapered optical fiber geometries and sensing applications based on mach- zehnder interferometer: a review, Opt. Fiber Technol. 58 (2020) 102302, https://doi.org/10.1016/j.yofte.2020.102302.

[20] Y. Huang, Z. Tian, L.P. Sun, D. Sun, J. Li, Y. Ran, B.O. Guan, High-sensitivity DNA biosensor based on optical fiber taper interferometer coated with conjugated polymer tentacle, Opt. Express 23 (21) (2015) 26962–26968, https://doi.org/10.1364/OE.23.026962.

[21] A. Pg, A. Xl, Z.A. Xue, A. Yz, C.A. Ning, A. Sw, Optical fiber sensors for glucose concentration measurement: a review, Opt. Laser Technol. 139 (2021) 106981, https://doi.org/10.1016/j.optlastec.2021.106981.

[22] D. Sun, Y. Fu, Y. Yang, Label-free detection of breast cancer biomarker using silica microfiber interferometry, Opt. Commun. 463 (2020) 125375, https://doi.org/10.1016/j.optcom.2020.125375.

[23] S. Hong, Y.S. Na, S. Choi, I.T. Song, W.Y. Kim, H. Lee, Non-Covalent Self-Assembly and Covalent Polymerization Co-Contribute to Polydopamine Formation, Adv. Funct. Mater. 22 (2012) 4711–4717, https://doi.org/10.1002/adfm.201201156.

[24] S. Hong, K.Y. Kim, H.J. Wook, S.Y. Park, K.D. Lee, D.Y. Lee, H. Lee, Attenuation of the in vivo toxicity of biomaterials by polydopamine surface modification, Nanomedicine 6 (5) (2011) 793–801, https://doi.org/10.2217/nnm.11.76.

[25] F. Emilie, F.D. Céline, J. Christine, L. Joël, F. David, W. Patrice, D. Christophe, Catechols as versatile platforms in polymer chemistry, Prog. Polym. Sci. 38 (1) (2013) 236–270, https://doi.org/10.1016/j.progpolymsci.2012.06.004.

[26] E.M. Martin, V. Del, Cyclodextrins and their uses: a review, Process Biochem. 39 (9) (2004) 1033–1046, https://doi.org/10.1016/S0032-9592(03)00258-9.

[27] V.T. Dsouza, K.B. Lipkowitz, Cyclodextrins: Introduction, Chem. Rev. 98 (5) (1998) 1741–1742, https://doi.org/10.1021/cr980027p.

[28] A. Zornoza, C. Martín, M. Sánchez, I. Vélaz, A. Piquer, Inclusion complexation of glisentide with α-, β- and γ-cyclodextrins, Int. J. Pharm. 169 (1998) 239–244, https://doi.org/10.1016/S0378-5173(98)00124-0.

[29] E. Christoforides, A. Papaioannou, K. Bethanis, Crystal structure of the inclusion complex of cholesterol in β-cyclodextrin and molecular dynamics studies, Beilstein J. Org. Chem. 14 (2018) 838–848, https://doi.org/10.3762/bjoc.14.69.

[30] J. Yao, T. Wu, Y. Sun, Z. Ma, M. Liu, Y. Zhang, S. Yao, A novel biomimetic nanoenzyme based on ferrocene derivative polymer NPs coated with polydopamine, Talanta 195 (2019) 265–271, https://doi.org/10.1016/j.talanta.2018.11.069.

[31] R.P. Liang, C.M. Liu, X.Y. Meng, J.W. Wang, J.D. Qiu, A novel open-tubular capillary electrochromatography using β-cyclodextrin functionalized graphene oxide-magnetic nanocomposites as tunable stationary phase, J. Chromatogr. A 1266 (2012) 95–102, https://doi.org/10.1016/j.chroma.2012.09.101.

[32] Y.X. Dai, J.F. Zhong, J.Q. Li, X. Liu, Y.H. Wang, Interaction mechanism of cholesterol/β-cyclodextrin complexation by combined experimental and computational approaches, Food Hydrocoll. 130 (2022) 107725, https://doi.org/10.1016/J.FOODHYD.2022.107725.

[33] A.M. Dehghani, G. Bahlakeh, B. Ramezanzadeh, A.H. Mofidabadi, Cyclodextrin-based nano-carrier for intelligent delivery of dopamine in a self-healable anti-corrosion coating, J. Environ. Chem. Eng. 105457 (2021), https://doi.org/10.1016/j.jece.2021.105457.

[34] Q. Wei, F. Zhang, J. Li, B. Li, C. Zhao, Oxidant-induced dopamine polymerization for multifunctional coatings, Polym. Chem. 1 (2010) 1430–1433, https://doi.org/10.1039/C0PY00215A.

[35] J. Nishijo, S. Moriyama, S. Shiota, Interactions of Cholesterol with Cyclodextrins in Aqueous Solution, Chem. Pharm. Bull. 51 (11) (2003) 1253–1257, https://doi.org/10.1248/cpb.51.1253.

[36] D. Schmitz, A. Pich, Responsive microgels with supramolecular crosslinks: synthesis and triggered degradation in aqueous medium, Polym. Chem. 7 (2016) 5687–5697, https://doi.org/10.1039/C6PY01039C.